Scientia Iranica, Vol. 11, Nos. 1&2, pp 37–49

SCIENTIA
IRANICA

Simulation of Detonation Initiation in Straight and Baffled Channels

M. Farshchi* **and S. Hossainpour**[1]

Euler conservation equations, ideal gas state equations and simplified chemical kinetics models were used to simulate two-dimensional straight and baffled shock tubes. In a straight channel, detonation waves were initiated by a strong shock wave and allowed to travel down the channel to reach a CJ wave condition. It has been shown that a two-step reaction, kinetics model with an induction time delay, resulted in a physically plausible transient solution. The one-step kinetics model solution is only valid at the limit of a steady state CJ wave condition and should not be used for transient problems. The two-step kinetics model was then used to simulate a detonation initiation in a baffled shock tube. It was shown that the presence of multiple baffles in a channel could result in an initiation of detonation, in cases where the temperature jump across the traveling initial compression wave and the presence of a single baffle are not sufficient to initiate a detonation. Furthermore, it is shown that in the absence of any viscous mechanisms, shock reflection from the second baffle created a moving Mach stem between the baffles. The coalescence and focusing of pressure waves behind this Mach stem resulted in the creation of a hot spot leading to a detonation wave.

INTRODUCTION

The study of shock wave propagation, in channels partially obstructed by baffles and wedges and filled with reacting mixture of gases, has applications in many industrial safety situations, as well as in mechanical operations such as pulsed detonation engines. The presence of any obstacles in the shock wave path could result in a detonation wave. Strehlow [1] has observed that even the presence of bumps and crevasses on straight channel walls, if large enough, can destroy the one-dimensional nature of the flow and lead to shock reinforcement and detonation initiation.

The use of wall obstacles to induce transition from deflagration to detonation was observed many years ago. The mechanism by which transition is facilitated has been credited to the generation of turbulence by the obstacles, hence, promoting flame acceleration [2]. However, more recent experiments by Chue et al. [3] have demonstrated that channel wall obstacles create transverse pressure waves whose interactions result in the formation and maintenance of a detonation wave. Furthermore, Chan has observed a complex interaction of shock waves between two obstacles resulting in the formation of a detonation wave [4]. Experiments of Chan have indicated that in stoichiometric hydrogen-oxygen mixtures, initiation of detonation can be achieved by the collision of a shock wave with obstacles, whereas the shock wave was not strong enough to initiate chemical reactions by itself.

The author's investigation is motivated by Chan observations [4]. Chan used a 9×9 cm, 4 m long shock channel with two, baffle-type obstacles mounted in the test section. The heights of these obstacles were 3.8 and 2.5 cm, respectively and they were mounted 20 cm apart from each other. A shock wave was generated in the gas mixture by breaking the shock channel's diaphragm with a plunger. Chan presented Schlieren photographs for the collision of a 2.2 Mach number shock wave with obstacles. The collision of the shock wave with the first obstacle did not cause ignition in the vicinity of the obstacle. However, as the transmitted shock wave continued to propagate downstream and collided with the second obstacle,

*. *Corresponding Author, Department of Aerospace Engineering, Sharif University of Technology, Tehran, I.R. Iran.*

1. *Department of Mechanical Engineering, Sharif University of Technology, Tehran, I.R. Iran.*

ignition of the mixture occurred near the upstream face of the second obstacle. The schlieren photographs indicated that the first obstacle caused the initially planar shock to diffract. Subsequent oblique collision of the diffracted shock with the bottom wall caused the formation of a Mach stem. The collision of the Mach stem with the second obstacle created a strong enough shock reflection to heat the gas mixture beyond its auto-ignition temperature, causing ignition. The schlieren photographs did not show clearly the formation of a flame kernel, however, Chan suggested that viscous dissipation along the slip surface behind the reflected Mach stem had heated the gas to higher temperature relative to its surroundings, causing a mild ignition.

Although viscous dissipations may be the actual cause of the ignition observed by Chan, there are also inviscid gas dynamic interactions, such as pressure wave focusing, which could create local hot spots capable of causing an ignition point in the mixture. This is not meant to underestimate the role of turbulent mixing and viscous dissipation in creating locally sensitive regions. In fact, both viscous and inviscid mechanisms are at work under normal circumstances. However, it is unclear whether inviscid gas dynamic effects alone could account for Chan's observations.

The objective of the present work is to address this issue and evaluate the possibility of detonation initiation due to pressure wave interactions in the absence of any viscous dissipation effects. Chan's experimental work has provided a suitable test case to distinguish between the contributions of viscous dissipation effects versus inviscid gas dynamics effects. His experiment was used to construct a computational model to determine if inviscid gas dynamic effects could result in detonation initiation in the case of a weak shock propagating in a channel with multiple obstacles.

To achieve this objective a computational tool for the study and analysis of detonation initiation and propagation in two-dimensional complex geometries was required. Experimental studies of the structure of detonation waves indicate that the leading shock front is found to consist of convex segments whose boundaries are not stationary but move across the detonation front as it advances [5]. At the boundaries of these segments, the shock front is broken discontinuously and additional gas dynamic processes extend from the intersection loci into the reaction zone region behind the primary shock front. Therefore, the structure of detonation waves is rather three-dimensional. However, to date, the majority of numerical simulations of the detonation initiation and propagation have been limited to two-dimensional models. This is due partly to computational limitations and partly to the fact that two-dimensional simulations have been able to capture the transverse structures that are the key component of the detonation structure [6]. The experimental setup and observations of Chan, which are used as the bases for the present numerical simulation, reinforce this assumption.

Numerical methods with monotone second order space and time differencing and accurate shock capturing capabilities have been developed. These methods have been used for the solution of chemically reacting high-speed flows with multiple discontinuity surfaces on structured and unstructured adaptive grids. Oran et al. [6] have performed high-resolution, two-dimensional computations of the propagation of a detonation in a diluted mixture of hydrogen and oxygen using Euler equations and a detailed chemical reaction mechanism. They examined the features of transverse waves and the cellular structure that develops behind a CJ wave. Bourlioux and Majda [7] presented numerical simulations of unstable two-dimensional detonations. They used a higher order Godunov scheme, adaptive mesh refinement and conservative front tracking to solve two-dimensional Euler equations with a simplified one step, chemical reaction model. Molecular transport effects were neglected in the above investigations and in many other numerical simulations of detonation waves. Since the time scales for diffusion transport processes are long, compared with convective and heat release time scales, molecular transport processes have a negligible effect.

A finite volume, upwind, inviscid flow solver has been developed for simulation of two-dimensional or axi-symmetric chemically reacting flows on an adaptive, square, unstructured grid. The flow solver has several features. Fluxes on cell faces are calculated using the Roe's flux-difference splitting method. Spatial accuracy is increased using gradients of the solution variables. The solution algorithm uses a cell-centered scheme with a mesh refinement method to adapt the mesh resolution in regions with large pressure or density gradients. The grid adaptive procedure involves mesh enrichment and coarsening by adding points in high gradient regions of the flow and by removing points where they are not needed. To increase the time accuracy of the method, a mid-point rule is used for the time integration.

The chemical reaction kinetics model is probably the most important physical model in the simulation of detonation initiation. The reduced kinetics model must be chosen carefully to prevent the initiation kinetic effects from being lost in the simulations. Experiments have shown that direct initiation of a detonation wave requires sufficient energy and power [8]. A sufficiently strong shock wave must be created and sustained for a sufficient period of time before detonation can follow. This observation points to the importance of chemical reaction kinetics, in general, and the reaction induction

time, in particular. In spite of this observation, many researchers have used simple one-step irreversible kinetics models in their work (see [7,9,10]). The justification for the use of these models is that while they provide a great deal of computational savings, a remarkable range of physical phenomena can be captured qualitatively if a few simple parameters, such as heat release, activation energy or precursor shock strength, are varied. However, as will be shown later, such simplification should be done selectively and only in special cases where the transient nature of the detonation initiation is not under scrutiny. To account for the reaction kinetics induction time, a two-step Arrhenius kinetics model is considered. In this reaction mechanism, two progress parameters are introduced to account for the induction time, as well as exothermic reactions [11,12].

Smirnov and Panfilov [13] used an irreversible, two-step kinetics model for simulation of the detonation initiation in a viscous, heat-conductive reactive mixture. They used an induction step and an exothermic step with equal rate constants and activation energies. Using this model, they investigated the range of activation energies where transition from deflagration to detonation can take place. They stated that lowering the activation energy to a certain limit, E=10 kcal/mole in their study, leads to the development of a strong detonation wave, almost instantly, that is coincident at the point of the shock formed by the forced ignition condition. They also pointed out that the strong detonation wave eventually slows down to the Chapman-Jouguet speed.

Several one-step and two-step kinetics models for the simulation of detonation initiation were examined. In straight channels, where detonation was initiated by a strong shock wave, a model similar to the Smirnov and Panfilov model was used. It was shown that a two-step reaction kinetics model resulted in a physically plausible transient solution. A one-step version of this model was shown to be only valid at the limit of a steady state CJ wave condition and could not be used for transient problems.

In the following sections, the governing equations, the numerical solution method and its validation, are discussed first. Next, the authors' findings are presented on the effects of one-step and two-step kinetics models on the evolution of a detonation wave and its approach to a CJ wave. Finally, the results on the initiation of detonation in a baffled shock tube are presented. Using a test case, based on Chan's experimental work it is shown that in the absence of molecular and turbulent diffusive and dissipative effects, multidimensional gas dynamic mechanisms, such as shock focusing, are capable of creating local hot spots causing a strong ignition leading to a detonation wave.

GOVERNING EQUATIONS

The governing equations are time dependent, two-dimensional or axi-symmetric Euler equations, describing an inviscid compressible flow of an ideal mixture of gases with a constant specific heat ratio. A two-step, irreversible, Arrhenius chemical reaction kinetics model is utilized. The two-step reaction model consists of an induction phase, measured by the decay of the parameter β from the initial value of one to the final value of zero, followed by an exothermic reaction phase, modeled by a single irreversible heat release parameter, λ. The heat release parameter is initially set to zero, resulting in zero chemical reaction heat release. It is activated after the induction time has elapsed, then it is allowed to grow and reach the maximum value of one at the completion of the heat release phase. The complete model, in a conservative form, is given as:

$$\frac{\partial(r^\alpha \mathbf{U})}{\partial t} + \frac{\partial(r^\alpha \mathbf{F})}{\partial x} + \frac{\partial(r^\alpha \mathbf{G})}{\partial r} = \mathbf{S}, \tag{1}$$

where α is zero for Cartesian coordinates and one for cylindrical coordinates. $\mathbf{U}, \mathbf{F}, \mathbf{G}$ and $\mathbf{S}$ are defined as follows:

$$\mathbf{U} = \begin{Bmatrix} \rho \\ \rho u \\ \rho v \\ \rho e_t \\ \rho\lambda \\ \rho\beta \end{Bmatrix}, \quad \mathbf{F} = \begin{Bmatrix} \rho u \\ \rho u^2 + P \\ \rho uv \\ \rho u(e_t + P/\rho) \\ \rho u\lambda \\ \rho u\beta \end{Bmatrix},$$

$$\mathbf{G} = \begin{Bmatrix} \rho v \\ \rho vu \\ \rho v^2 + P \\ \rho v(e_t + P/\rho) \\ \rho v\lambda \\ \rho v\beta \end{Bmatrix}, \quad \mathbf{S} = \begin{Bmatrix} 0 \\ 0 \\ \alpha P \\ 0 \\ \rho\omega_\lambda \\ \rho\omega_\beta \end{Bmatrix}, \tag{2}$$

$$\omega_\lambda = k_\lambda(1-\lambda)\exp(-E_\lambda \rho/P)\chi(\beta),$$

$$\chi(\beta) = \begin{cases} 0 & \beta > 0 \\ 1 & \beta \le 0 \end{cases}, \tag{3}$$

$$\omega_\beta = -k_\beta \exp(-E_\omega \rho/P), \tag{4}$$

$$P = (\gamma - 1)\left[\rho e_t - \frac{1}{2}\rho(u^2 + v^2) + \rho\lambda q\right]. \tag{5}$$

Here, u and v are the longitudinal and transverse components of the velocity vector, respectively. The variables γ, P, ρ and e_t represent the specific heat ratio, pressure, density and total energy per unit mass, respectively. Also, q is the heat of reaction per unit mass, k_λ, k_β and E_λ, E_β are the forward

reaction rate constants and activation energy per unit mass for exothermic reactions and induction time delay, respectively.

NUMERICAL METHOD

The choice of a numerical method is dictated by the complex structure and time dependent dynamics of the detonation wave, as well as the complexity of the two dimensional geometrical domain of the problem. The detonation wave can be characterized by its fast moving shock front (of negligible thickness) followed by a narrow, heat releasing, reaction zone which supports the shock motion. Any geometrical complexity, such as varying cross sectional area or the presence of obstacles, creates highly complicated wave interactions. The numerical technique should, thus, be capable of capturing shocks without any oscillations and with minimum added numerical diffusion. The numerical method used in this work is based on the high-resolution scheme on a Cartesian adaptive-mesh presented by Chiang [14].

Spatial Discretization

A finite volume, upwind scheme, based on Roe's flux-difference splitting method, on an adaptive square unstructured grid, is employed here. The conservative finite volume form of the governing transport equations can be obtained by integrating these equations over a cell area, Ω, and application of Gauss' theorem.

$$\iint_{\Omega} \mathbf{U}_t dA + \oint_{\partial\Omega} (\mathbf{F}dy - \mathbf{G}dx) = \iint_{\Omega} \mathbf{S}dA. \tag{6}$$

The surface integrals are expressed in terms of the average value of state variables over the cell, while the line integral becomes a sum of the fluxes over the four faces of the quadrilateral cell as follows:

$$A\frac{d\overline{\mathbf{U}}}{dt} + \sum_{k=1}^{4} (\mathbf{F}^k(\Delta X)_k + \mathbf{G}^k(\Delta Y)_k) = A\overline{\mathbf{S}}. \tag{7}$$

Here, A is the area of the cell and a bar represents an average quantity in a cell. The fluxes $\mathbf{F}^k$ and $\mathbf{G}^k$ are average values on the cell face, k. Introducing the cell face length, Δs, the above equation can be rewritten as:

$$A\frac{d\overline{\mathbf{U}}}{dt} + \sum_{k=1}^{4} \mathbf{F}_{\perp}^k \Delta s_k = A\overline{\mathbf{S}}, \tag{8}$$

where $\mathbf{F}_{\perp}$ is the flux normal to the cell face (see Figure 1):

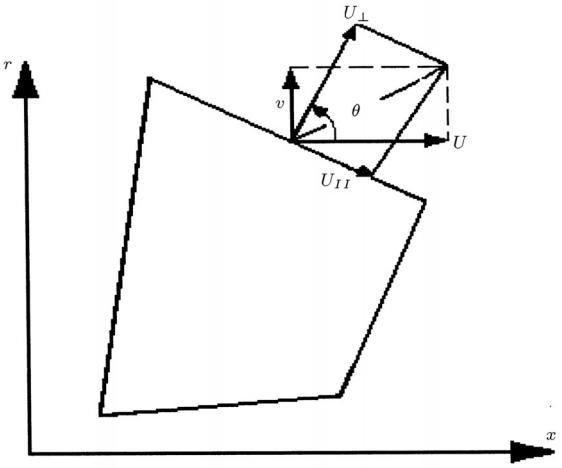

Figure 1. Geometry for normal flux calculation.

$$\mathbf{F}_{\perp} = \begin{Bmatrix} \rho u_{\perp} \\ \rho u_{\perp} u + P\cos\theta \\ \rho u_{\perp} v + P\sin\theta \\ \rho u_{\perp}(e_t + P/\rho) \\ \rho u_{\perp}\lambda \\ \rho u_{\perp}\beta \end{Bmatrix},$$

$$\cos\theta = \frac{\Delta y}{\Delta s},\ \sin\theta = \frac{\Delta x}{\Delta s},\ u_{\perp} = u\cos\theta + v\sin\theta. \tag{9}$$

Next, the numerical flux function, based on Roe's approximate Riemann solution, can be used to determine needed flux values at cell faces [15]. The flux across a cell face, of which the normal is at an angle, θ, with respect to the x-axis, is computed from the following equation:

$$\mathbf{F}(\mathbf{U}_L, \mathbf{U}_R) = \frac{1}{2}(\mathbf{F}(\mathbf{U}_L) + \mathbf{F}(\mathbf{U}_R)) - \frac{1}{2}\sum_{k=1}^{6} \left|\tilde{\mathbf{a}}^k\right| \Delta\mathbf{V}^k \tilde{\mathbf{R}}^k, \tag{10}$$

where L (left) and R (right) refer to the lower and higher cell index, respectively. The eigenvalue vector, $\tilde{\mathbf{a}}$, is composed of the characteristic speeds and the matrix, $\tilde{\mathbf{R}}$, is composed of the right eigenvectors of the mean value flux Jacobian matrix:

$$\tilde{\mathbf{a}} = \begin{Bmatrix} \tilde{u}_{\perp} - \tilde{c} \\ \tilde{u}_{\perp} \\ \tilde{u}_{\perp} \\ \tilde{u}_{\perp} + \tilde{c} \\ \tilde{u}_{\perp} \\ \tilde{u}_{\perp} \end{Bmatrix},$$

$$\tilde{\mathbf{R}} = \begin{Bmatrix} 1 & 0 & 1 \\ \tilde{u} - \tilde{c}\cos\theta & -\tilde{c}\sin\theta & \tilde{u} \\ \tilde{v} - \tilde{c}\sin\theta & \tilde{c}\cos\theta & \tilde{v} \\ \tilde{h} - \tilde{u}_\perp c & \tilde{u}_{II} & \frac{1}{2}(\tilde{u}^2 + \tilde{v}^2) \\ \tilde{\lambda} & 0 & \frac{1}{2}\tilde{\lambda} \\ \tilde{\beta} & 0 & \frac{1}{2}\tilde{\beta} \end{Bmatrix}$$

$$\begin{matrix} 1 & 0 & 0 \\ \tilde{u} + \tilde{c}\cos\theta & 0 & 0 \\ \tilde{v} + \tilde{c}\sin\theta & 0 & 0 \\ \tilde{h} + \tilde{u}_\perp \tilde{c} & -q & 0 \\ \tilde{\lambda} & \cos\theta & \sin\theta \\ \tilde{\beta} & \sin\theta & \cos\theta \end{matrix} \Bigg\}. \tag{11}$$

The superscript tilde ($\sim$) refers to the so-called Roe average. The Roe average of a quantity is computed by weighting with $\sqrt{\rho}$, for instance, as shown in the following equation:

$$\tilde{\rho} = \sqrt{\rho_L}\sqrt{\rho_R}, \qquad \eta = \frac{\sqrt{\rho_L}}{\sqrt{\rho_L} + \sqrt{\rho_R}},$$

$$\tilde{u} = \eta u_L + (1-\eta)u_R, \qquad \tilde{v} = \eta v_L + (1-\eta)v_R,$$

$$\tilde{h} = \eta h_L + (1-\eta)h_R, \qquad \tilde{\lambda} = \eta\lambda_L + (1-\eta)\lambda_R,$$

$$\tilde{\beta} = \eta\beta_L + (1-\eta)\beta_R. \tag{12}$$

The other quantities with superscript tildes are not averaged independently, but are obtained from the basic Roe averaged quantities by their normal functional relation. The vector, $\Delta\mathbf{V}$, is given as:

$$\Delta\mathbf{V} = \begin{Bmatrix} \frac{\Delta P - \tilde{\rho}\tilde{c}\Delta u_\perp}{2\tilde{c}^2} \\ \frac{\tilde{\rho}\Delta u_{II}}{\tilde{c}} \\ \Delta\rho - \frac{\Delta P}{\tilde{c}^2} \\ \frac{\Delta P + \tilde{\rho}\tilde{c}\Delta u_\perp}{2\tilde{c}^2} \\ \tilde{\rho}\Delta\lambda + \frac{1}{2}\tilde{\lambda}(\Delta\rho - \frac{\Delta P}{\tilde{c}^2}) \\ \tilde{\rho}\Delta\beta + \frac{1}{2}\tilde{\beta}(\Delta\rho - \frac{\Delta P}{\tilde{c}^2}) \end{Bmatrix}$$

$$\Delta() = ()_L - ()_R. \tag{13}$$

Second Order Spatial Scheme

High gradient slip lines (caused by moving Mach stems), as well as inviscid separation points over the shock tube obstacles, create regions with high velocity and temperature gradients. These high gradient regions are perpendicular to the principle direction of gas motion in the shock tube. Application of first order spatial differencing introduces large amounts of numerical viscosity, which could result in artificial dissipation. This would lead to creation of unintended and nonphysical hot spots in high Mach number flow fields. To avoid this problem, higher order spatial differencing must be considered. Barth [16] has introduced a version of Van Leer's MUSCL algorithm, based on a linear reconstruction of the solution inside cells. High order accuracy in space is achieved by using interpolated flow values in each cell face using the known gradient of these values. This method can be shown as:

$$\mathbf{U}(r) = \mathbf{U}(r) + \nabla\mathbf{U} \bullet (r - r_0)\phi, \tag{14}$$

where r and r_0 refer to cell face and cell center, respectively. The special flux limiter, ϕ, is used to prevent numerical instabilities near shock regions.

Adaptive Unstructured Mesh Generation

The diversity of time and length scales present in our problem makes it very time consuming to reach physically meaningful results with a stationary uniform grid resolution. Therefore, a locally adaptive grid is used to resolve the flow field in the high gradient regions. Adaptive mesh methods attempt to increase the resolution in the region of necessity and can dramatically reduce the computational effort, especially in unsteady calculations [17]. The concept of the hierarchical cell-based quadtree, where a "parent" cell is refined by dividing it into four "children" cells, is introduced to construct the basic grid system. This structure treats the embedded grid as separate levels, as shown in Figure 2. However, the numerical calculations take place only on the cells without children; the parent values can be obtained by virtue of the children values.

This refinement procedure can be continued to several levels, until the required local resolution is reached. By removing children cells, one can recoarsen the mesh. The adaptive grid resolution technique used here is fully discussed by Chiang [14]. In the present study, the gradient of density, as well as the gradient

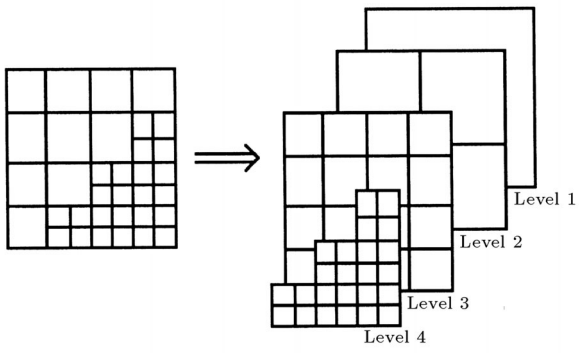

Figure 2. Cell refinement method.

of pressure, are used as the measure for flagging cell refinement.

Time Discretization

It is generally agreed that second order accuracy in time is required for the efficient solution of transient flow problems. An explicit, multi-stage, time marching approach with the mid-point rule is used here to achieve second order, accurate time integration. The Mid-Point rule is a two-stage technique given as:

$$\mathbf{U}^{n+\frac{1}{2}} = \mathbf{U}^n + \frac{\Delta t}{2}\mathrm{Res}(\mathbf{U}^n),$$

$$\mathbf{U}^{n+1} = \mathbf{U}^n + \Delta t\ \mathrm{Res}(\mathbf{U}^{n+\frac{1}{2}}), \qquad (15)$$

where $\mathrm{Res}(\mathbf{U})$ is a discretization of the spatial differential operator in the Euler equation.

The principle of time adaptation is to use two small time steps on the fine mesh, in order to keep up with one time step on a mesh twice as coarse. This is essentially applicable on a uniform grid and, in order to apply it, the cell next to the boundary of the fine-cell region must be divided into two equal cells. Sub-cell averages in the left and right half of the coarse cell need to be reconstructed. The first step in this reconstruction is to average the state vector in two fine cells near the boundary, in order to obtain a coarse-cell average in the fine-cell region. This is then used in combination with the data in the adjacent coarse cells to get a state-vector profile by interpolation. Once this profile is available, one can reconstruct sub-cell averages by integrating over sub-cells. The update from time 0 to time Δt on a coarse mesh corresponds to updating to two cycles of $1/2\Delta t$ on the fine mesh. By the same procedures of reconstructing and updating, the fine grid can be updated over another fine-grid time step, so that both grids end up at the same final time. Thus, accurate values are obtained on both coarse and fine grids. After this has been achieved, the coarse cell bordering the fine grid must be corrected in value to restore conservation in time. The difference between the flux integrals used for the fine cell and for the coarse cell at their interface must be applied to the coarse cell. Details of the multi-stage time marching and its adaptation to the mesh refinement technique used here can be found in Chiang [14].

Flow Solver Validation

The accuracy of a compressible flow solver is measured by its ability to capture discontinuity surfaces. The challenge in simulating unsteady flows is that these discontinuities are not stationary in the domain of solution and stationary grid clustering could not be used. When adaptive meshes and time steps are used in unsteady calculations, the moving cells on the boundary of fine and coarse meshes require additional spatial and temporal interpolations, which produces numerical errors not present in a uniform grid simulation. Therefore, if the solution results on an adaptive grid are comparable to those on a high-resolution uniform grid, then the goal of adaptive method has been achieved.

To validate the performance of the adaptive mesh Euler solver described above, two classical tests are utilized: A one-dimensional shock tube problem and a supersonic channel flow over a forward facing step.

The classical, one-dimensional shock tube problem has an exact solution with important features such as a shock wave, a contact discontinuity and an expansion fan. The two-dimensional flow solver was applied to a shock tube 3 m long with a partition at the middle of the tube. The gas on both sides of the partition is initially at rest. The pressure and density at the left side of the partition, $0 \leq x < 1.5$, are 1.0 Pa and 1.0 kg/m^3 and on the other side, $1.5 \leq x \leq 3.0, 0.1$ Pa and 0.125 kg/m^3, respectively. Figure 3 compares the exact solution of this problem to the two-dimensional, adaptive grid solution with three levels of refinement. The shock wave is accurately captured; however, some numerical diffusion is noticed around the contact discontinuity. The corresponding grid resolution pattern is shown at the bottom of Figure 3 with mesh refinement in the high gradient regions. Grid refinement is maintained on the left side of the shock tube partition due to the presence of the expansion fan. However, as the shock wave and contact discontinuity move out of a region on the right side of the partition, local higher level grids are removed and the mesh recoarsens.

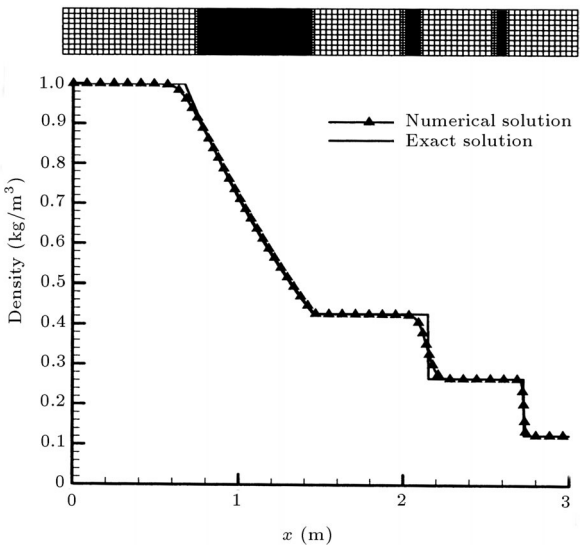

Figure 3. 2D-shock tube adaptive grid solution with four levels of refinement.

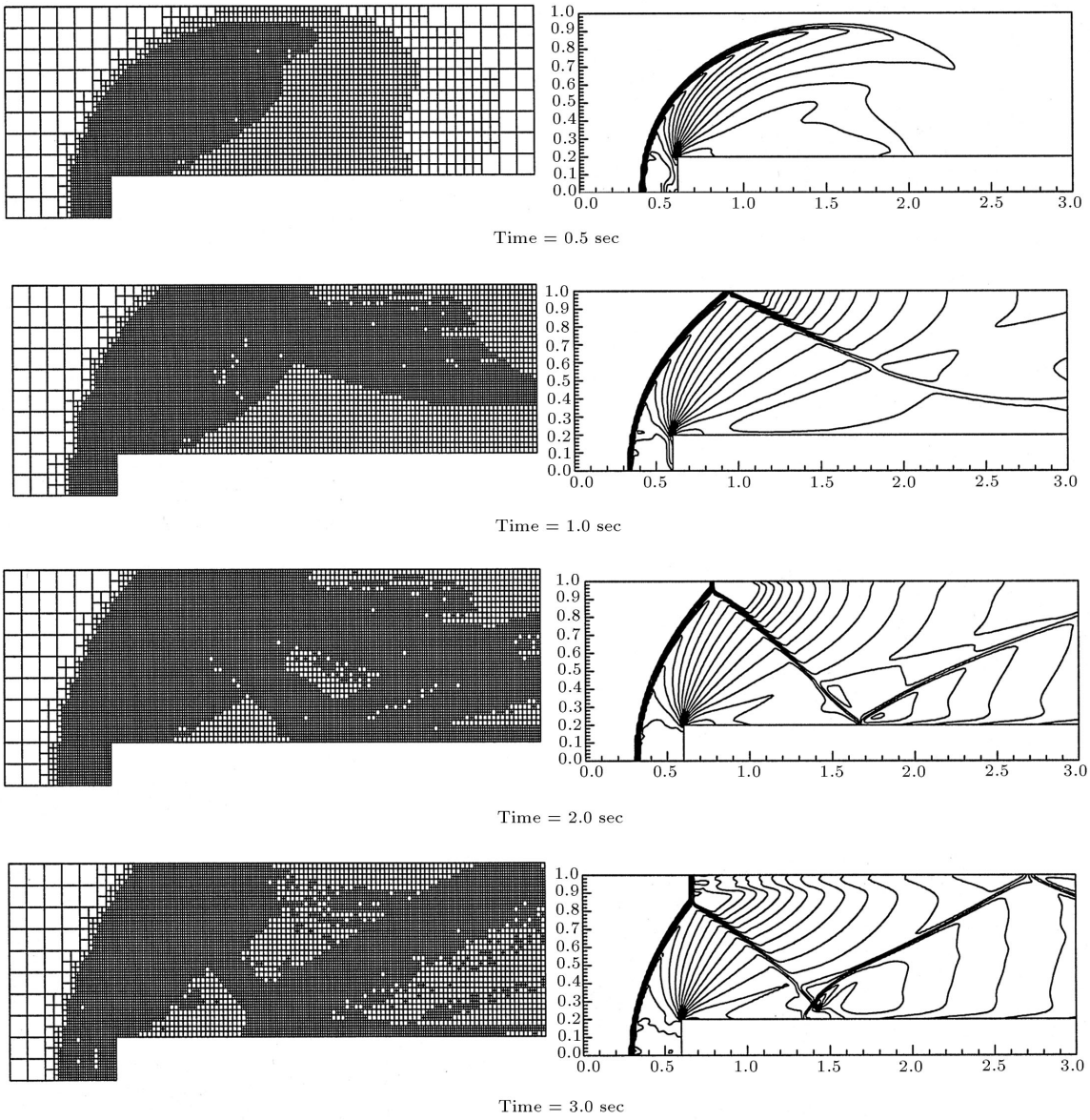

Figure 4. Time evolution of density contours and mesh refinements in the channel.

Non-reacting supersonic channel flow over a forward facing step is a two-dimensional numerical test case that has been studied intensively in the past. First introduced by Emery and later used by Van Leer and Woodward and Colella to compare a variety of numerical schemes for computing two-dimensional fluid flow with strong shocks [18,19], here, this test problem is used to validate the numerical scheme, as well as the grid adaptation producer. The problem involves a Mach 3 flow in a channel containing a step. The channel is one unit wide and three units long. The step is 0.2 units high and located 0.6 units from the entrance of the channel. The test problem begins with a uniform Mach 3 flow initial condition over the entire domain of the solution. Specified uniform, in-flow boundary conditions are used at the left boundary and "out flow" conditions are used at the exit boundary on the right. At the walls of the channel, reflecting boundary conditions are applied. Initially, the channel is filled with a gas which has 1.4 kg/m^3 density, 1.0 Pa pressure, 3 m/s velocity and $\gamma = 1.4$. Woodward and Colella [19] have presented the time evolution of the density distribution in the channel at half second time intervals, up to 4 seconds. They used the PPM numerical method on a uniform 240 $\times$ 80 grid with no local mesh clustering. In the present work, gradient of density is used as the measure for flagging mesh refinement and three levels of grid refinement are allowed on an initially 30 $\times$ 10 uniform grid. Therefore, the finest cell size in the present work is equal to the cell size used in their work. Figure 4 shows that the mesh refinement

and coarsening adapt well to the flow field density variations.

A comparison of these results with the results of Woodward and Colella [19], indicates that the present scheme is capable of accurately and efficiently capturing transient details of the flow field, such as shock reflection and Mach stem formation, as the flow field evolves with time. Based on these results, the flow solver was deemed valid for application to detonation problems.

RESULTS AND DISCUSSIONS

The effect of simplified chemical kinetics models on the initiation of a detonation wave and its approach to a Chapman-Jouguet wave in a straight channel will be discussed first. Next, initiation of a detonation wave in a channel with obstacles will be examined.

Effects of Reaction Induction Time Delay

A simplified, two-step reaction kinetics model is used to introduce exothermic chemical reactions, as well as an induction time delay into the combustion model. The two-step kinetics model used in the present study is similar to that of Smirnov and Panfilov [13]. The energy release per unit mass of mixture is $q = 2\times10^6$ J/kg and the activation energy and the reaction rate constant for the exothermic step are $E_\lambda = 10^6$ J/kg and $k_\lambda = 0.5 \times 10^6$ 1/sec, respectively. For the induction time step, the activation energy is $E_\beta = 10^6$ J/kg and the reaction rate constant is $k_\beta = 0.8 \times 10^6$ 1/sec.

To determine the effect of reaction induction time on the structure and development of a detonation wave, a 3.5 m long channel was considered. A diaphragm, located at 1.5 m from the left wall, divided the channel into two sections. The high-pressure section, on the left, was filled with a hot gas at 3.0×10^6 Pa pressure and 2.35 kg/m^3 density. The low-pressure section was filled with a combustible gas mixture at 10^5 Pa pressure and 1.2 kg/m^3 density. The ratio of specific heat capacities was assumed to be constant at $\gamma = 1.4$. Initially, the gas velocity on both sides of the partition was zero. Figure 5 presents the time evolution of density, temperature and pressure profiles along the channel for cases of chemical reaction with induction time delay (a), and no induction time delay (b). To realize the second case, the induction time parameter, β, was initially set to zero, causing the release of chemical energy as soon as calculations began (see Equations 2,3 and 5). Figure 6 shows the steady state structure of the detonation wave, one millisecond after precursor shock wave initiation, for the above cases. A millisecond after the precursor shock wave initiation, a Chapman-Jouguet detonation wave, with the steady state speed of 2037 m/sec, was established in both cases. However, there are major differences in the approach to the final structure of the resulting Chapman-Jouguet detonation waves. Figure 5 indicates that peak values of pressure and density behind the shock wave, were higher for the case of the chemical reaction with an induction time delay. However, the detonation front moved faster in the no-delay case. To explain these differences, the chemical energy release behind the precursor shock and the structure of the detonation wave must be examined. The effect of the chemical reaction induction time on the structure of the steady state detonation wave can be clearly seen in Figure 6. The detonation wave front has traveled about 5 mm more in the no-delay case, indicating that the average speed of the detonation front was slightly higher in this case. The application of the one-step reaction model (no-delay case) is physically equivalent to assuming that the time interval required for molecular collisions, resulting in the initiation of chemical reactions and subsequent heat release, is zero and reactions start instantaneously, as soon as the precursor shock passes over an unburned premixed gas.

Therefore, the small increase in the average speed of the detonation front is due to immediate energy release right after initial shock propagation into the combustible gas mixture. Comparison of axial density and pressure profiles, 60 microseconds after the shock initiation (Figure 5), indicates that there was much less energy release for the case with reaction delay.

The steady state structure of the detonation wave presented in Figure 6a shows that the reaction induction time delay allows for a gas dynamic jump due to the passage of the leading shock, followed by the increase, due to the chemical reaction energy release. Such a distinction cannot be made in the no-delay case (Figure 6b) and, hence, lower values of peak pressure and density exist behind the shock front.

The value of the heat release parameter, λ, was used to determine the instantaneous location of the detonation wave and its thickness. This information was then used to obtain the time history of the detonation wave propagation speed and the pressure behind the detonation wave, i.e. at the point where $|1 - \lambda| < 0.001$. Time histories of the detonation wave speed and its backpressure are presented in Figure 7. The final steady state values of detonation wave speed and backpressure are the same in both cases and are consistent with the CJ wave properties under the above initial conditions. However, Figure 7 shows that for the case with reaction induction time delay, the shock wave has gone through a short transient phase. Within about 160 microseconds after its initiation, it exceeded the CJ wave speed, becoming a strong detonation wave. It then reached its maximum speed at about

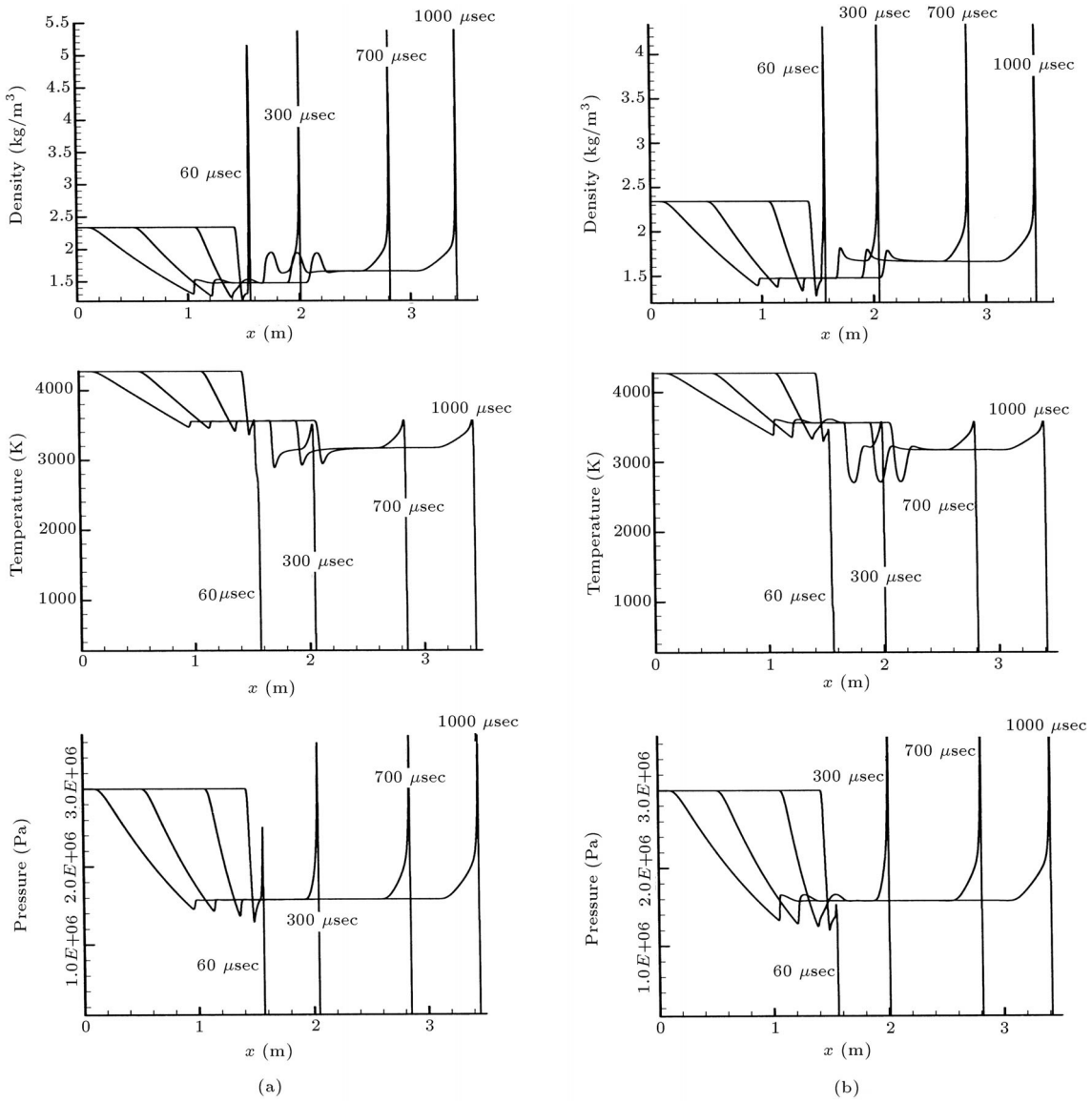

Figure 5. Time evolution of density, temperature and pressure distribution with (a) and without (b) induction time.

200 microseconds and then, gradually, relaxed to a CJ wave with a terminal speed of 2037 m/sec. For the no-delay case, the instantaneous detonation velocity value was always below the steady state CJ wave speed and, gradually, approached the CJ value. This behavior is physically unacceptable, since the CJ wave speed is the minimum detonation speed possible. Therefore, the solution to the detonation wave problem with no chemical reaction induction time delay is only valid at the limit of steady state and cannot be used for transient calculations.

Detonation Initiation in a Baffled Channel

Clearly, the Chan experiment could not be simulated with its complete chemical, physical and geometrical complexity. Therefore, it was decided to create a model problem that would maintain some of the main features of his experiment and allow the authors to conduct numerical experiments and simulate detonation caused by the collision of a relatively weak shock wave with multiple obstacles. To do this, a two-dimensional channel, 25 cm long and 3 cm wide, was considered. The channel was divided into two sections. The left section was 3.5 cm long and filled with a compressed inert gas at a pressure of 1.19179×10^6 Pa and a density of 4.86 kg/m^3. To simulate plunger action and also save on computational effort by keeping the size of the driver compartment small, this gas was given an initial uniform velocity of 827.6 m/sec. The right section was fitted with two baffle-type obstacles. The first obstacle was 1.2 cm high and placed 5 cm from the left boundary and the second obstacle was 1 cm high and placed 10 cm from the left boundary. This section

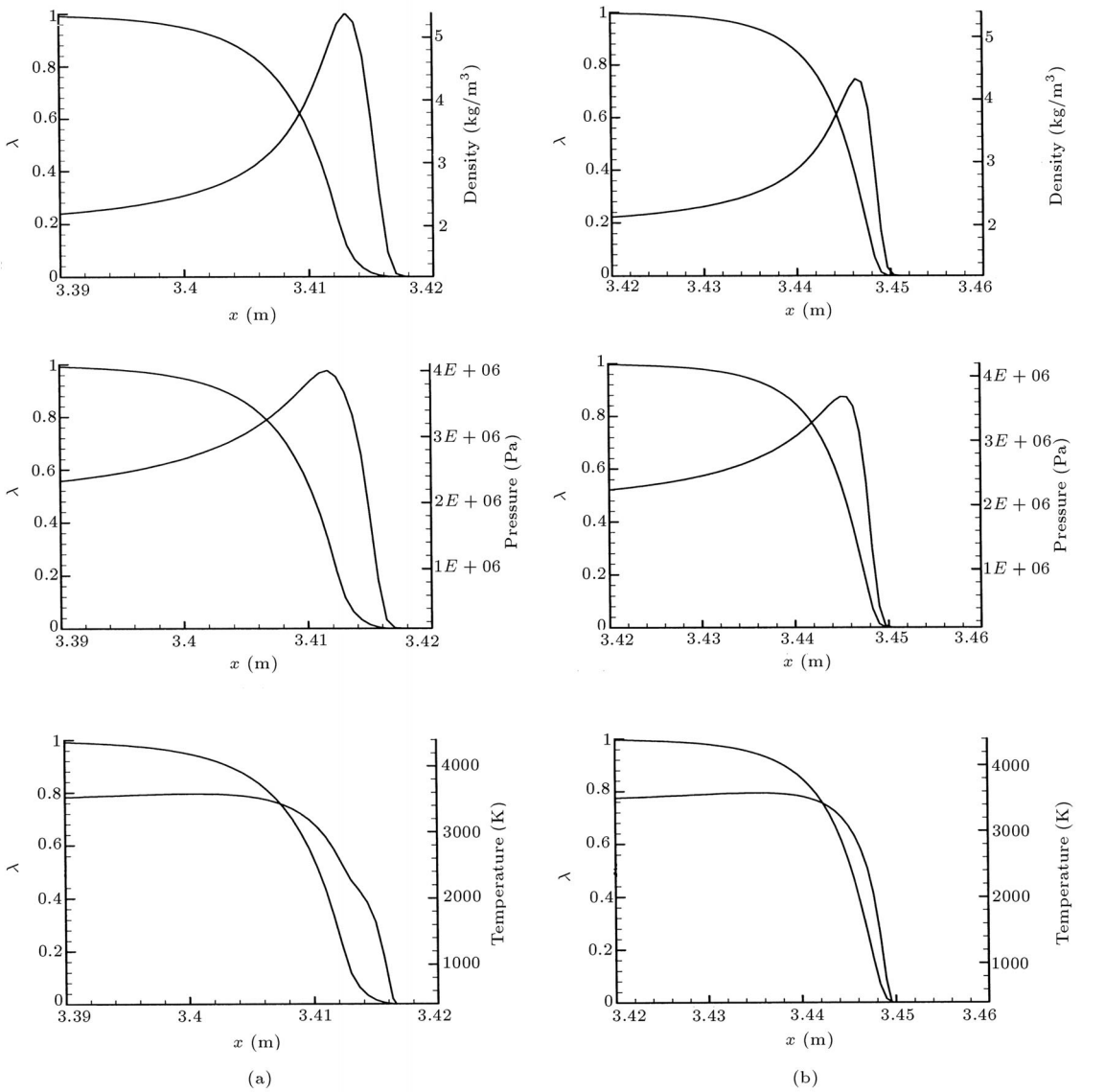

Figure 6. Density, temperature and pressure distribution with (a) and without (b) induction time.

was filled with a combustible gas mixture at a pressure of 1.0×10^5 pa, a density of 1.2 kg/m^3 and with zero initial velocity. Euler conservation equations, ideal gas state equations and the simplified, two-step, chemical kinetics model presented above were used to simulate the two-dimensional baffled shock channel. The values used for the reaction kinetics model parameters and the gas energy releases were those presented above. The auto-ignition temperature of the combustible gas mixture was set to 1500 K. Given the above activation energy and reaction rate constant for the induction delay equation, approximately 12 μsec of ignition time delay is expected at this auto-ignition temperature.

The finite volume, second-order, upwind flow solver described above was used on an adaptive square unstructured grid to solve the governing equations. The computational platform used for these calculations was a Pentium III PC with a 750 MHz processor and 256 Meg RAM. Each run took about 20 hours and the maximum number of grid points was limited by the computer memory size. The numerical domain was initially sub-divided into a uniform mesh of 320×38 (12160) square cells. The mesh was then refined as the shock wave propagated in the region. Only one level of refinement was allowed, because greater refinement levels increase cell numbers beyond the available computer memory. The final mesh had 51070 cells, of which only 12160 were in the initial level.

Figure 8 presents ten frames of density and temperature contours for the flow field, as the incident shock wave propagates down the channel and collides with obstacles. The second frame of Figure 8 indicates that the incident shock wave diffracted after collision with the first obstacle and a Mach stem was created

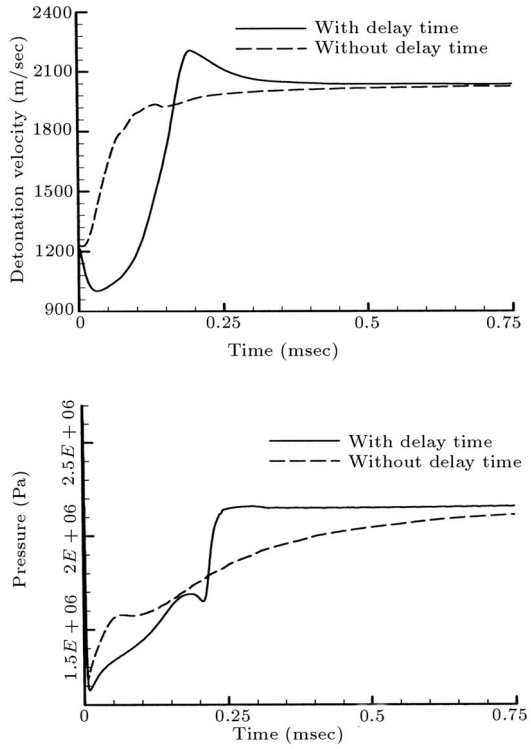

Figure 7. Time histories of detonation velocity and backpressure.

upon collision of the diffracted oblique shock wave with the bottom surface of the channel. The third and forth frames show that the traveling Mach stem and the related oblique shock collided with the second obstacle and created two shock waves. One was diffracted off the obstacle and became an oblique shock wave colliding with the bottom surface of the channel, forming a Mach stem moving downstream. The other one was a reflected shock wave that became oblique and formed a Mach stem moving upstream back into the shock-heated gas. Temperature contours of the fourth frame ($t = 95.9$ μsec) indicate that there was a chemical reaction and a high heat release region on the upstream side of the second obstacle. This was the region most intensely heated by the reflected shock, increasing its temperature over the gas auto-ignition temperature. The second baffle partially blocked blast waves created by the chemical reactions in this corner region from propagating downstream and reinforcing the original incident shock wave. However, these blast waves can easily propagate upstream, reinforcing the oblique shock and the Mach stem moving into the preheated gas. The temperature contours of the fifth frame ($t = 105.5$ μsec) show that the coalescence and focusing of these blast waves behind the reflected oblique shock created an intense region of high temperature chemical reactions. The density and temperature contours of the remaining frames show that the reflected oblique shock wave and related Mach stem became stationary almost half way between the two baffles and a large region, downstream of it, was exploded into chemical reactions.

Temperature contours in frames seven to ten show that a strong reaction front was formed. This front collided with the top channel wall and propagated downstream, approaching the original incident shock wave. Figure 9 presents the axial values of temperature and density at $t = 142.9$ μsec along the channel mid plane, showing the formation of a detonation wave.

The onset of detonation observed above is similar to the strong ignition detonation initiation described by Meyer and Oppenheim [20], whereas Chan [14] suggests appearance of flame kernels or "spotty" ignition along the slip surface behind the Mach stem, leading to a mild ignition. Since molecular transport effects are neglected in our formulation and inviscid Euler equations are used, one could not directly check the importance of the viscous dissipation effects. However, using a first order upwind difference scheme would result in numerical dissipation, which acts similar to real molecular dissipation. It is interesting to note that when a first order differencing scheme was used for the solution of the above problem, a high temperature reacting region appeared around the slip line of the upstream moving Mach stem and the dynamics of detonation initiation were changed by the appearance of a large reaction region before any pressure wave coalescence could create a hot spot behind the upstream moving oblique shock. This is mentioned only as a caveat and, since these observations were based on numerical dissipation, which is grid and time dependent, such results are not presented here.

Even though the above results are only qualitatively comparable with the experimental observations of Chan, they indicate that a numerical simulation with simplified but sufficient chemical reaction and physical models can provide insight into the dynamics of the detonation phenomenon that is not easily accessible through experimental observations.

CONCLUSION

A finite volume, second-order accurate, upwind adaptive, unstructured-grid, inviscid flow solver for simulation of two-dimensional or axi-symmetric chemical reacting flow fields has been developed. Exothermic chemical reactions, as well as an induction time delay, are introduced in the combustion model using a simplified two-step reaction kinetics mechanism. This flow solver is shown to be capable of capturing major physical effects in stationary and transient supersonic flow fields with relatively complex geometry. Numerical simulations of initiation and propagation of detonation waves in straight and baffled channels are performed. First, a shock channel is simulated by initiating a

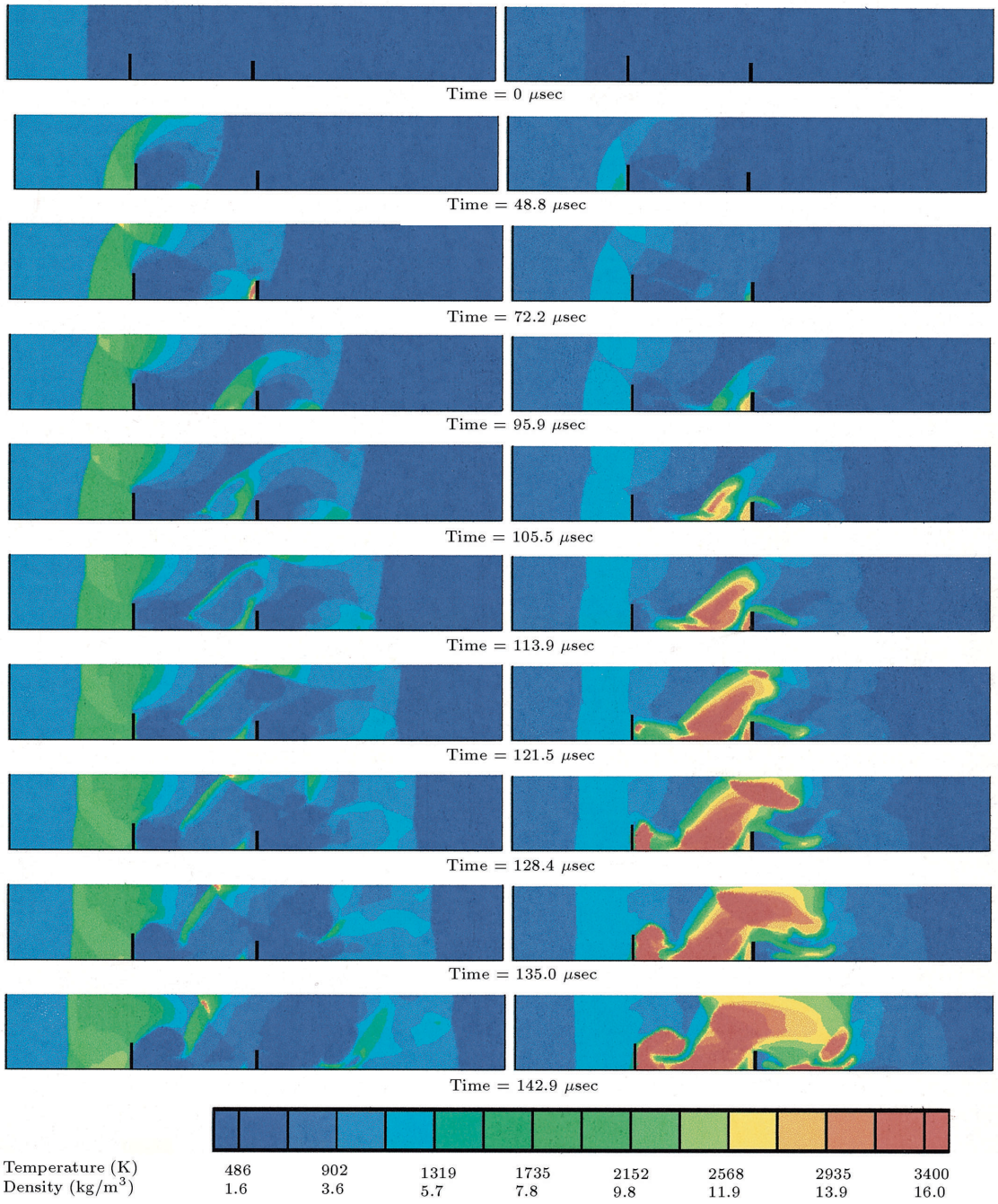

Figure 8. Density and temperature contours of collision of a shock wave with obstacles.

strong detonation wave and allowing it to travel down the channel to reach a CJ wave condition. It is shown that a two-step reaction kinetics model, accounting for the reaction induction time delay, is a minimum requirement to obtain a physically plausible transient solution. A one-step reaction kinetics model results in a detonation wave whose transient speed is always less than the CJ wave speed and approaches this value only at steady state. Next, the unsteady propagation of a relatively weak shock wave in a two-dimensional channel partially obstructed by two consecutive baffles and filled with a combustible mixture of gases has been considered. The results are qualitatively consistent with experimental observations of Chan [4] and show local heating and reaction initiation caused by shock reinforcement upstream of the second baffle. This shock reinforcement region is created by the coalescence and focusing of pressure waves behind a reflected oblique shock and Mach stem moving upstream into the shock-heated gas mixture. A series of numerical simulations can be easily performed to evaluate the effects of the channel and baffle geometrical characteristics upon ini-

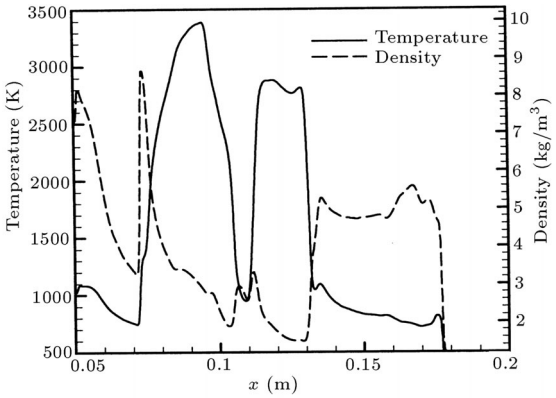

Figure 9. Axial density and temperature profiles at the channel mid-plane at $t = 142.9$ μsec.

tiation of the detonation wave. Preliminary simulations indicate that the distance between the baffles for a channel with a fixed height is a key parameter in local shock reinforcement and detonation initiation. These results are encouraging and point to the capability of analyzing this flow field in more detail.

ACKNOWLEDGEMENT

The financial support of the Sharif University of Technology is gratefully acknowledged.

REFERENCES

1. Strehlow, R.A., *Combustion Fundamentals*, McGraw-Hill, New York (1984).
2. Lee, J.H.S. "Fast flame and detonations", in *The Chemistry of Combustion Processes, American Chemical Society Symposium Series 249*, Washington, D.C., pp 119-150 (1984).
3. Chue, R.S., Lee, J.H., Scarinci, T., Papyrin, A. and Knystautas, R. "Transition from fast deflagration to detonation under the influence of wall obstacles", *AIAA Progress in Astronautics and Aeronautics*, **153**, pp 270-282 (1993).
4. Chan, C.K. "Collision of a shock wave with obstacles in a combustible mixture", *Combustion and Flame*, **100**, pp 341-348 (1995).
5. Schott, G.L. "Observations of the structure of spinning detonation", *Physics of Fluids*, **8**(5), pp 850-865 (1965).
6. Oran, E.S., Weber, Jr. J.W., Stefaniw, E.I., Lefebvre, M.H. and Anderson, Jr. J.D. "A numerical study of a two-dimensional H_2-O_2-Ar detonation using a detail chemical reaction model", *Combustion and Flame*, **113**, pp 147-163 (1998).
7. Bourlioux, A. and Majda, A.J. "Theoretical and numerical structure for unstable two-dimensional detonations", *Combustion and Flame*, **90**, pp 211-229 (1992).
8. Lee, J.H.S. "Initiation of gaseous detonation", *Annual Review of Phys. Chem.*, **28**, pp 75-104 (1977).
9. Clarke, J.F., Kassoy, D.R. and Riley, N. "On the direct initiation of a plane detonation wave", *Proc. Roy. Soc. Lond. A*, **408**, pp 129-148 (1986).
10. Clarke, J.F., Karni, S., Quirk, J.J., Roe, P.L., Simmonds, L.G. and Toro, E.F. "Numerical simulation of two-dimensional unsteady detonation waves in high energy solids", *Journal of Computational Physics*, **106**, pp 215-233 (1993).
11. Takano, Y. "Simulations for detonation initiation behind reflected shock waves", *Dynamic Aspects of Detonations, AIAA Progress in Astronautics and Aeronautics*, **153**, pp 283-297 (1993).
12. Taki, S. and Fujiwara, T. "Numerical simulation on the establishment of gaseous detonation", *Dynamics of Detonations and Explosions, AIAA Progress in Astronautics and Aeronautics*, **94**, pp 186-200 (1984).
13. Simirnov, N.N. and Panfilov, I.I. "Deflagration to detonation transition in combustible gas mixtures", *Combustion and Flame*, **101**, pp 91-100 (1995).
14. Chiang, Y.L. "Simulation of unsteady inviscid flow on an adaptively refined cartesian grid", Ph.D. thesis, Department of Mechanical Engineering, University of Michigan, USA (1991).
15. Roe, P.L. "Approximate Reimann solvers, parameter vectors and difference schemes", *Journal of Computational Physics*, **43**, pp 357-372 (1981).
16. Barth, T.J. "On unstructured grids and solvers", in *Computational Fluid Dynamics*, Von Karman Institute for Fluid Dynamics, Lecture Series 1990-04 (1990).
17. Powell, K.G., Roe, P.L. and Quirk, J., *Adaptive-Mesh Algorithms for Computational Fluid Dynamics* (1991).
18. Van Leer, B. "Towards the ultimate conservation difference scheme V. A second order sequel to Godunov's method", *Journal of Computational Physics*, **32**, pp (1979).
19. Woodward, P. and Colella, P. "The numerical simulation of two-dimensional fluid flow with strong shocks", *Journal of Computational Physics*, **54**, pp 115-173 (1984).
20. Meyer, J.W. and Oppenheim, A.K. "On the shock-induced ignition of explosive gases", *Thirteen Symposium (International) on Combustion*, pp 1153-1164 (1970).